
UNDERSTANDING MULTIMODAL CONTRASTIVE LEARNING THROUGH POINTWISE MUTUAL INFORMATION

Toshimitsu Uesaka

Sony AI
Tokyo, Japan
toshimitsu.uesaka@sony.com

Taiji Suzuki

The University of Tokyo, RIKEN AIP
Tokyo, Japan
taiji@mist.i.u-tokyo.ac.jp

Yuhta Takida & Chieh-Hsin Lai & Naoki Murata

Sony AI
Tokyo, Japan
{yuta.takida, chieh-hsin.lai, naoki.murata}@sony.com

Yuki Mitsufuji

Sony AI, Sony Group Corporation
Tokyo, Japan
yuhki.mitsufuji@sony.com

ABSTRACT

Multimodal representation learning to integrate different modalities, such as text, vision, and audio is important for real-world applications. The symmetric InfoNCE loss proposed in CLIP is a key concept in multimodal representation learning. In this work, we provide a theoretical understanding of the symmetric InfoNCE loss through the lens of the pointwise mutual information and show that encoders that achieve the optimal similarity in the pretraining provide a good representation for downstream classification tasks under mild assumptions. Based on our theoretical results, we also propose a new similarity metric for multimodal contrastive learning by utilizing a nonlinear kernel to enrich the capability. To verify the effectiveness of the proposed method, we demonstrate pretraining of multimodal representation models on the Conceptual Caption datasets and evaluate zero-shot classification and linear classification on common benchmark datasets.

1 INTRODUCTION

CLIP (Radford et al., 2021) and ALIGN (Jia et al., 2021) established one of the most common frameworks for multimodal representation learning (Guo et al., 2019). In this framework, to obtain the vision-language representation, two encoders that map inputs from different modalities onto a shared space are trained with a contrastive loss (Chopra et al., 2005). Recent studies have shown that a CLIP model pretrained on a large-scale text-image dataset provides transferable features to various downstream tasks such as linear classification (Radford et al., 2021; Jia et al., 2021), text-to-video retrieval (Lin et al., 2022), text-conditioned image generation (Ramesh et al., 2022), and manipulation (Patashnik et al., 2021). Recent works have shown that a CLIP model can be used to feed vision information to large language models (Alayrac et al., 2022). In addition to the text and vision modalities, this multimodal contrastive learning framework can be applied to other combinations of modalities such as text-audio representations (Elizalde et al., 2023). Furthermore, some works have shown that a shared representation over more than two modalities can be obtained by bridging two modalities with the contrastive framework repeatedly or simultaneously (Guzhov et al., 2022; Wu et al., 2022; Girdhar et al., 2023).

Despite the success of CLIP models in various empirical applications, the theoretical understanding of why the CLIP model is so effective in downstream tasks is still limited. Saunshi et al. (2019) showed guarantees on the performance of downstream classifications for representations obtained by contrastive learning. However, their guarantees rely on the strong assumption of conditional

independence of two samples in paired data. Although subsequent works have mitigated this issue (HaoChen et al., 2021; Tosh et al., 2021; Wang et al., 2022; Huang et al., 2023; Waida et al., 2023), those works still have one of the following issues to understand the framework of CLIP. First, some works provided only upper bounds of downstream losses and didn't consider how close the upper bounds are to the optimal one. Second, some works set the target of theoretical analysis to their own proposed method that is different from the actual setting of CLIP. Last, some works assumed the settings of contrastive learning in a single modality that differs from the case of CLIP.

In this paper, we provide a new understanding of the contrastive loss used in the framework of CLIP, which we call the symmetric InfoNCE loss, through the lens of the pointwise mutual information. More precisely, we spotlight the fact that maximization of the symmetric InfoNCE loss is achieved when the similarity between two features in the loss is equal to the pointwise mutual information of the two data up to a constant. Moreover, we show that the optimal (possibly nonlinear) classifier in downstream classification tasks can be constructed by a linear classifier when the similarity between two features indicates the pointwise mutual information under some assumptions. Our theoretical results solve the three issues above.

Based on our theoretical analysis of the symmetric InfoNCE, we propose a new class of similarities that has more representation power than the cosine similarity, which is the bilinear similarity in the latent space. We construct the similarities by utilizing a nonlinear kernel and sets of points, which leads to richer capability. To demonstrate the effectiveness of the proposed method, we conduct experiments on text-image datasets.

In summary, our main contributions are as follows:

- We provide a theoretical analysis of the performance of representations obtained by multi-modal contrastive learning through the lens of the pointwise mutual information. We show that, in downstream classifications, a linear classifier close to the optimal (possibly nonlinear) classifier can be constructed when the optimal similarity of the symmetric InfoNCE is obtained.
- Based on our theoretical results, we propose a new class of similarities for contrastive learning to reduce the gap between the optimal similarity and actual similarities obtained in the pretraining. We construct the similarity based on a nonlinear kernel and sets of points.
- We demonstrate the performance of our proposed method with empirical results of text-image representation learning on CC3M and CC12M.

2 RELATED WORK

2.1 MULTIMODAL CONTRASTIVE REPRESENTATION LEARNING IN PRACTICE

CLIP (Radford et al., 2021) and ALIGN (Jia et al., 2021) proposed to use contrastive loss to obtain vision-language representation, inspired by a series of studies of deep metric learning and unimodal contrastive learning such as multi-class N-pair loss (Sohn, 2016), InfoNCE (Oord et al., 2018), SimCLR (Chen et al., 2020), and ConVIRT (Zhang et al., 2022). Both works showed the success of pretrained models with large-scale paired datasets and the contrastive loss, which we call the symmetric InfoNCE in this paper, in zero-shot settings and downstream tasks.

Following the success of this contrastive framework, various works have extended this vision-language representation learning framework by combining other losses, for example, by using masked language modeling and image-text matching (Li et al., 2021a; 2022), by using image captioning (Yu et al., 2022), and by imposing additional constraints on representation (Goel et al., 2022; Mu et al., 2022). In those works, the symmetric InfoNCE still plays an important role. Not limited to vision-language representation, this contrastive learning framework has been applied to other domains (Guzhov et al., 2022; Wu et al., 2022; Elizalde et al., 2023; Girdhar et al., 2023).

Another approach to extending this contrastive framework is modifying the similarity in the symmetric InfoNCE loss. Fürst et al. (2022) proposed to use modern Hopfield networks to enrich the structure of the similarity, while also replacing the InfoNCE with the InfoLOOB. Desai et al. (2023) proposed to use the Lorentzian distance in a hyperbolic space as the similarity to capture a hierarchy structure of visual and linguistic concepts. We adopt this approach and propose to enrich the class of the

similarity based on a nonlinear kernel and sets of points. Different to these studies, we provide an error analysis of features produced by the proposed method in downstream classification tasks.

2.2 THEORETICAL UNDERSTANDING OF CONTRASTIVE LOSS

Early works attributed the success of the InfoNCE loss (Oord et al., 2018) to the fact that the InfoNCE is a lower bound of mutual information and the optimization of the InfoNCE leads to maximization of mutual information between two views of data (Hjelm et al., 2019; Bachman et al., 2019; Tian et al., 2020). However, Tschannen et al. (2020) showed that maximizing tighter bounds on mutual information can result in worse representations with a thought experiment and empirical results. Li et al. (2021b) also showed that representations that have the same mutual information can have different qualities. Instead of the perspective from mutual information, Wang & Isola (2020) brought a perspective from alignment and uniformity to understand the InfoNCE. This idea has affected subsequent works on theoretical analysis of contrastive learning (Li et al., 2021b; Zimmermann et al., 2021; Huang et al., 2023).

Regarding the theoretical relationship to downstream tasks, Saunshi et al. (2019) showed that the downstream classification loss is upper bounded by a quantity monotonically increasing with respect to the contrastive loss. Although Saunshi et al. (2019) relied on the strong assumption of conditional independence of two samples, subsequent studies have mitigated this problem. HaoChen et al. (2021) proposed the spectral contrastive loss and provided an upper bound of the linear probe performance based on the augmentation graph. Tosh et al. (2021) analyzed the excess loss of linear predictors on the landmark embedding from the perspective of multi-view redundancy. Wang et al. (2022) showed upper and lower bounds for downstream performance through the conditional feature variance and the augmentation overlap effect. Ash et al. (2022) investigated upper bounds of a supervised loss in terms of the number of negative samples. Huang et al. (2023) analyzed the performance of the nearest neighbor classifier through the (σ, δ) -augmentation. Shi et al. (2023) investigated the trade-off between label efficiency and universality under assumptions of linear data. Waida et al. (2023) proposed the kernel contrastive loss and showed an upper bound of the classification error.

However, we argue that there are still three issues to understand the framework of CLIP. First, some works provided only upper bounds of downstream losses. If there is a certain gap between the upper bounds and the optimal value, reducing the contrastive loss does not always mean better performance in the downstream task. Second, some works changed the target of theoretical analysis from the actual setting of CLIP or the InfoNCE. Some works provided guarantees on their proposed losses or different features from usual contrastive learning. Last, some upper or lower bounds included the statistics, e.g., variance, of obtained presentations. Those bounds are useful when the perfect alignment is achieved. However, the perfect alignment is not practical in the case of multimodal learning where paired samples are not generated by augmentations of the same instance and a data sample in a modality has relationship to many samples in the other modality.

Our work differs from those works in the following ways. First, we consider not only an upper bound of the performance but also the gap from the optimal classifier. Second, we analyze the symmetric InfoNCE and linear classifiers that are constructed by a way close to the actual setting of CLIP. Last, our assumptions for theoretical results are relatively mild in the case of multimodal representation learning, which is explained in Section 4.2.

3 PROBLEM SETUP

In this section, we introduce notations and problem settings that we use in our theoretical analysis. In Section 3.1, we formalize the multimodal contrastive representation learning. In Section 3.2, we formalize the downstream linear classification task, which is commonly used to evaluate contrastive learning methods (Chen et al., 2020; Radford et al., 2021).

3.1 CONTRASTIVE REPRESENTATION LEARNING AND THE SYMMETRIC INFONCE

Let \mathcal{X} and \mathcal{Y} denote the input space of two modalities. For the sake of simplicity, we focus on text-image representation learning, and we denote the image space by \mathcal{X} and the text space by \mathcal{Y} . Note that \mathcal{X} and \mathcal{Y} can be replaced with any modality. Let $\mathcal{D}_{\mathcal{X} \times \mathcal{Y}}$ denote the joint data distribution

over $\mathcal{X} \times \mathcal{Y}$. Let $\mathcal{D}_{\mathcal{X}}$ and $\mathcal{D}_{\mathcal{Y}}$ denote the marginal data distribution over \mathcal{X} and \mathcal{Y} , respectively. Let $p(x, y), p(x)$ and $p(y)$ denote the density of $\mathcal{D}_{\mathcal{X} \times \mathcal{Y}}, \mathcal{D}_{\mathcal{X}}$ and $\mathcal{D}_{\mathcal{Y}}$, respectively. For a probability density function p , we denote the support of the probability as $\text{supp } p$. Given a batch of N image-text pairs $(x_1, y_1), \dots, (x_N, y_N) \sim \mathcal{D}_{\mathcal{X} \times \mathcal{Y}}$, CLIP (Radford et al., 2021) introduced the following contrastive loss to train an image encoder $f_{\mathcal{X}}: \mathcal{X} \rightarrow \mathbb{R}^d$, a text encoder $f_{\mathcal{Y}}: \mathcal{Y} \rightarrow \mathbb{R}^d$ and a trainable temperature parameter $\tau \in \mathbb{R}_{>0}$.

$$\hat{\mathcal{L}}(f_{\mathcal{X}}, f_{\mathcal{Y}}, \tau) = \frac{1}{2} \left[-\frac{1}{N} \sum_{i=1}^N \ln \frac{\exp(f_{\mathcal{X}}(x_i)^\top f_{\mathcal{Y}}(y_i)/\tau)}{\sum_{k=1}^N \exp(f_{\mathcal{X}}(x_k)^\top f_{\mathcal{Y}}(y_i)/\tau)} - \frac{1}{N} \sum_{i=1}^N \ln \frac{\exp(f_{\mathcal{X}}(x_i)^\top f_{\mathcal{Y}}(y_i)/\tau)}{\sum_{k=1}^N \exp(f_{\mathcal{X}}(x_i)^\top f_{\mathcal{Y}}(y_k)/\tau)} \right]. \quad (1)$$

We call it the symmetric InfoNCE loss. By minimizing the symmetric InfoNCE loss, the similarity of two features from paired samples (x_i, y_i) is expected to get larger, and the similarity of two features from independent samples x_i and y_j ($i \neq j$) is expected to get smaller. Here, the similarity of two features is measured by the cosine similarity $f_{\mathcal{X}}(x)^\top f_{\mathcal{Y}}(y)$. Note that the features $f_{\mathcal{X}}(x)$ and $f_{\mathcal{Y}}(y)$ are usually normalized such that they lie on the unit sphere.

Following the asymptotic form of the InfoNCE in Wang & Isola (2020), we consider the population expectation form of the symmetric InfoNCE. By considering the limit as $N \rightarrow \infty$, we have the population expectation form of the symmetric InfoNCE:

$$\mathcal{L}(f_{\mathcal{X}}, f_{\mathcal{Y}}, \tau) = \frac{1}{2} \mathbb{E}_{(x,y) \sim \mathcal{D}_{\mathcal{X} \times \mathcal{Y}}} \left[-\ln \frac{\exp(f_{\mathcal{X}}(x)^\top f_{\mathcal{Y}}(y)/\tau)}{\mathbb{E}_{x' \sim \mathcal{D}_{\mathcal{X}}} [\exp(f_{\mathcal{X}}(x')^\top f_{\mathcal{Y}}(y)/\tau)]} \right] + \frac{1}{2} \mathbb{E}_{(x,y) \sim \mathcal{D}_{\mathcal{X} \times \mathcal{Y}}} \left[-\ln \frac{\exp(f_{\mathcal{X}}(x)^\top f_{\mathcal{Y}}(y)/\tau)}{\mathbb{E}_{y' \sim \mathcal{D}_{\mathcal{Y}}} [\exp(f_{\mathcal{X}}(x)^\top f_{\mathcal{Y}}(y')/\tau)]} \right], \quad (2)$$

where we omit the constant term that comes from $\ln N$. Furthermore, we reformulate this by introducing a general similarity function $g: \mathcal{X} \times \mathcal{Y} \rightarrow \mathbb{R}$ of two samples $(x, y) \in \mathcal{X} \times \mathcal{Y}$ as follows:

$$\mathcal{L}_{\text{NCE}}(g) = \frac{1}{2} \mathbb{E}_{(x,y) \sim \mathcal{D}_{\mathcal{X} \times \mathcal{Y}}} \left[-\ln \frac{\exp g(x, y)}{\mathbb{E}_{x' \sim \mathcal{D}_{\mathcal{X}}} [\exp g(x', y)]} \right] + \frac{1}{2} \mathbb{E}_{(x,y) \sim \mathcal{D}_{\mathcal{X} \times \mathcal{Y}}} \left[-\ln \frac{\exp g(x, y)}{\mathbb{E}_{y' \sim \mathcal{D}_{\mathcal{Y}}} [\exp g(x, y')] } \right]. \quad (3)$$

When we set the similarity as $g(x, y) = f_{\mathcal{X}}(x)^\top f_{\mathcal{Y}}(y)/\tau$, Eq. 3 is equivalent to Eq. 2.

3.2 DOWNSTREAM CLASSIFICATION TASK

As a common evaluation of the learned representations with the symmetric InfoNCE, we consider a supervised classification task with K labels. Define $[M] := \{1, \dots, M\}$. Let $P(c|x)$ be the conditional distribution of the label $c \in [K]$ given the data $x \in \mathcal{X}$. We define $p(x, c) = P(c|x)p(x)$ as the density of the joint distribution of data x and its label c . We assume that pairs of data and its label, (x, c) , can be drawn from $p(x, c)$. In this supervised learning setting, a classifier $h: \mathcal{X} \rightarrow \mathbb{R}^K$ is often trained by minimization of the softmax cross-entropy loss given by

$$\mathcal{L}_{\text{sup}}(h) := \mathbb{E}_{p(x,c)} \left[-\ln \frac{\exp h(x)_c}{\sum_{i=1}^K \exp h(x)_i} \right], \quad (4)$$

where $h(x)_i$ denotes the i -th element of $h(x) \in \mathbb{R}^K$. In downstream linear classifications after the contrastive learning, h is constructed as a linear classifier over the learned representation. Given the encoder $f_{\mathcal{X}}$, we formalize this linear classifier as follows:

$$h(x; f_{\mathcal{X}}) := W^\top f_{\mathcal{X}}(x) + b, \quad (5)$$

where $W \in \mathbb{R}^{d \times K}$ is a weight and $b \in \mathbb{R}^K$ is a bias. With this $h(x; f_{\mathcal{X}})$, the downstream classification task is formalized as the minimization problem of \mathcal{L}_{sup} with respect to W and b :

$$\min_{W \in \mathbb{R}^{d \times K}, b \in \mathbb{R}^K} \mathcal{L}_{\text{sup}}(h(x; f_{\mathcal{X}})). \quad (6)$$

4 THEORETICAL GUARANTEE VIA POINTWISE MUTUAL INFORMATION

In this section, we upper bound the performance of downstream classification tasks. In Section 4.1, we review that the optimal similarity of the symmetric InfoNCE loss is represented by the pointwise mutual information. In Section 4.2, we show that if the optimal similarity is obtained, there is a linear classifier on the learned representation that is close to the optimal (possibly nonlinear) classifier. In Section 4.3, we investigate an error caused by the deviation from the optimal similarity.

4.1 POINTWISE MUTUAL INFORMATION AS THE OPTIMAL SIMILARITY

Our analysis starts with the following fact shown by Zhang et al. (2023) that the optimal similarity of the symmetric InfoNCE is represented by the pointwise mutual information.

Proposition 4.1 (Restatement of Proposition 1 in Zhang et al. (2023)). *Let X and Y denote two random variables having the joint probability density p . Then, the mutual information of X and Y , $I(X, Y) := \mathbb{E}_{p(x,y)} \left[\ln \frac{p(x,y)}{p(x)p(y)} \right]$ is an upper bound of $-\mathcal{L}_{\text{NCE}}(g)$. Moreover, if the function g satisfies*

$$g(x, y) = \ln \frac{p(x, y)}{p(x)p(y)} + C,$$

for a constant $C \in \mathbb{R}$, then the equality $I(X, Y) = -\mathcal{L}_{\text{NCE}}(g)$ holds.

In other words, when we consider the minimization problem of $\mathcal{L}_{\text{NCE}}(g)$ in terms of the measurable function g over $\mathcal{X} \times \mathcal{Y}$, the optimal similarity is equal to the pointwise mutual information up to a constant. Let denote this optimal similarity by $g^*(x, y) := \ln \frac{p(x,y)}{p(x)p(y)} + C$ for some $C \in \mathbb{R}$.

4.2 POINTWISE MUTUAL INFORMATION ESTIMATOR LEADS TO A GOOD LINEAR CLASSIFIER

Next, we consider the situation where we successfully get encoders that achieve the optimal similarity $g^*(x, y) = f_{\mathcal{X}}^*(x)^\top f_{\mathcal{Y}}^*(y)/\tau^*$ in the contrastive learning phase. We show that, under some conditions, a linear classifier over the learned representation can be close to the optimal classifier $h^* = \arg \min_h \mathcal{L}_{\text{sup}}(h)$.

It is known that the log probability of the label c conditioned by data x is the minimizer of \mathcal{L}_{sup} up to a constant because \mathcal{L}_{sup} is represented by using the cross entropy $H(\cdot, \cdot)$ as follows:

$$\mathcal{L}_{\text{sup}}(h) = \mathbb{E}_{p(x)} [H(P(c|x), Q(c|x))], \quad (7)$$

where we define $Q(c|x) := \frac{\exp h(x)_c}{\sum_{i=1}^K \exp h(x)_i}$. This is minimized when $P(c|x) = Q(c|x)$ for $x \in \text{supp } p(x)$. Thus, we have $h^*(x)_i = \ln P(i|x) + C'$ with a constant $C' \in \mathbb{R}$.

In the following, we demonstrate how to construct a linear classifier that is close to this optimal (possibly nonlinear) classifier h^* . First, we consider K disjoint subsets of the other domain, \mathcal{Y}_i ($i = 1, \dots, K$) $\subseteq \mathcal{Y}$, i.e., for $i \neq j$, $\mathcal{Y}_i \cap \mathcal{Y}_j = \emptyset$. Let $\tilde{\mathcal{Y}} = \mathcal{Y}_1 \cup \mathcal{Y}_2 \cup \dots \cup \mathcal{Y}_K$. Note that $\tilde{\mathcal{Y}}$ is not necessarily equal to \mathcal{Y} . We define $P(\mathcal{Y}_i) := P(y \in \mathcal{Y}_i)$. We assume that $P(\mathcal{Y}_i) \neq 0$ for every i . We define the conditional probability of y given \mathcal{Y}_i as follows:

$$p(y|\mathcal{Y}_i) := \begin{cases} p(y)/P(\mathcal{Y}_i) & \text{if } y \in \mathcal{Y}_i, \\ 0 & \text{if } y \notin \mathcal{Y}_i. \end{cases} \quad (8)$$

We notice that $p(y|\mathcal{Y}_i)$ is a probability density function on \mathcal{Y} (i.e., $\int_{y \in \mathcal{Y}} p(y|\mathcal{Y}_i) dy = 1$) which corresponds to the conditional distribution of y conditioned by \mathcal{Y}_i . Given the disjoint subsets, $\{\mathcal{Y}_i\}_{i \in [K]}$, and the components of similarity $g(x, y) = f_{\mathcal{X}}(x)^\top f_{\mathcal{Y}}(y)/\tau$, we construct a linear classifier on the representation $\bar{h}^g(x) = \bar{W}^\top f_{\mathcal{X}}(x) + \bar{b}$ as follows:

$$\begin{aligned} \bar{W} &:= [\bar{w}_1, \bar{w}_2, \dots, \bar{w}_K] \in \mathbb{R}^{d \times K}, \\ \bar{w}_i &:= \mathbb{E}_{p(y|\mathcal{Y}_i)} \left[\frac{1}{\tau} f_{\mathcal{Y}}(y) \right] \in \mathbb{R}^d, \\ \bar{b} &:= [\ln P(\mathcal{Y}_1), \ln P(\mathcal{Y}_2), \dots, \ln P(\mathcal{Y}_K)]^\top \in \mathbb{R}^d. \end{aligned}$$

Regarding the linear classifier on the representation that achieves the optimal similarity of the symmetric InfoNCE, $\bar{h}^{g^*}(x)$, we have the following upper bound on the risk of the downstream task.

Theorem 4.2. *Assume that $g^*(x, y) := \frac{1}{\tau^*} f_{\mathcal{X}}^*(x)^\top f_{\mathcal{Y}}^*(y) = \ln \frac{p(x, y)}{p(x)p(y)} + C$ holds for some $C \in \mathbb{R}$ and for any $x \in \text{supp } p(x) \subseteq \mathcal{X}$ and any $y \in \tilde{\mathcal{Y}}$. Then, for any choice of the decomposition $(\mathcal{Y}_i)_{i=1}^K$, it holds that*

$$\mathcal{L}_{\text{sup}}(\bar{h}^{g^*}) - \mathcal{L}_{\text{sup}}(h^*) \leq \mathbb{E}_{p(x)} \left[D_{\text{KL}} \left(P(c|x) \parallel P(\mathcal{Y}_c|x, \tilde{\mathcal{Y}}) \right) \right] + \mathbb{E}_{p(x, c)} [D_{\text{KL}}(p(y|\mathcal{Y}_c) \parallel p(y|x, \mathcal{Y}_c))], \quad (9)$$

where $P(\mathcal{Y}_c|x, \tilde{\mathcal{Y}}) := \frac{P(y \in \mathcal{Y}_c|x)}{P(y \in \tilde{\mathcal{Y}}|x)}$ and $p(y|x, \mathcal{Y}_c) := \frac{p(y|x)}{P(y \in \mathcal{Y}_c|x)}$ if $y \in \mathcal{Y}_c$, otherwise 0.

The proof is provided in Section B.1. Theorem 4.2 says that a similarity equal to the pointwise mutual information (up to a constant) leads to a linear classifier close to h^* if there exist subsets $\{\mathcal{Y}_c\}_{c \in [K]}$ such that the conditional probability $P(y \in \mathcal{Y}_c|x)$ is almost proportional to the conditional probability of label $P(c|x)$ and y is almost independent of x inside \mathcal{Y}_c .

Remark. We claim that this assumption on the existence of good subsets is not strong in the case of text-image representation learning and that this has a relationship to the prompt ensembling in the zero-shot classification. In zero-shot classification, Radford et al. (2021) proposed to ensemble embeddings of prompt templates such as “a photo of a {label}” and “a blurry photo of a {label}” for construction of a classifier of the labels. Since the set of prompt templates for each label shares the information except for the label, the probability of each set should be almost proportional to the probability of the label. In addition, the prompt templates lack most of information specific to images. Thus, each prompt in the set can be considered to be almost independent of images. Furthermore, we note that ensembling over the set of prompts can be considered as an approximation of the expectation over $p(y|\mathcal{Y}_i)$, which appears in the construction of the weight of \bar{h}^g .

4.3 ERROR ANALYSIS IN TERMS OF THE GAP FROM THE POINTWISE MUTUAL INFORMATION

We have observed that a similarity equal to the pointwise mutual information up to a constant leads a good classifier that is close to the optimal classifier in the downstream classification. However, an actual similarity obtained in the pretraining, $g(x, y)$, is possibly different from $g^*(x, y)$ because of the non-convexity of the optimization problem and the insufficient representational capability of the class of similarity, $\{(x, y) \mapsto f_{\mathcal{X}}(x)^\top f_{\mathcal{Y}}(y)/\tau \mid f_{\mathcal{X}}(x), f_{\mathcal{Y}}(y) \in \mathbb{R}^d, \tau \in \mathbb{R}_{>0}\}$. To consider the effect of a gap in the similarity, we decompose the risk of the downstream task as follows:

$$\mathcal{L}_{\text{sup}}(\bar{h}^g) - \mathcal{L}_{\text{sup}}(h^*) = \left(\mathcal{L}_{\text{sup}}(\bar{h}^g) - \mathcal{L}_{\text{sup}}(\bar{h}^{g^*}) \right) + \left(\mathcal{L}_{\text{sup}}(\bar{h}^{g^*}) - \mathcal{L}_{\text{sup}}(h^*) \right). \quad (10)$$

The second term in RHS of Eq. 10 is already bounded by Theorem 4.2. About the first term, we have the following bound.

Lemma 4.3. *Assume that, there exists $\Delta \geq 0$ such that $|g(x, y) - g^*(x, y)| \leq \Delta$ for all $x \in \text{supp } p(x)$ and all $y \in \text{supp } p(y)$. Then, it holds that $|\mathcal{L}_{\text{sup}}(\bar{h}^g) - \mathcal{L}_{\text{sup}}(\bar{h}^{g^*})| \leq 2\Delta$.*

The proof is provided in Section B.2. From Theorem 4.2, Lemma 4.3 and the fact that $\min_{W \in \mathbb{R}^{d \times K}, b \in \mathbb{R}^K} \mathcal{L}_{\text{sup}}(W^\top f_{\mathcal{X}}(\cdot) + b) \leq \mathcal{L}_{\text{sup}}(\bar{h}^g)$, we have the following result.

Theorem 4.4. *Assume that there exist K disjoint subsets \mathcal{Y}_i ($i = 1, \dots, K$) $\subseteq \mathcal{Y}$ such that*

$$\begin{aligned} D_{\text{KL}} \left(p(c|x) \parallel p(\mathcal{Y}_c|x, \tilde{\mathcal{Y}}) \right) &\leq \varepsilon_1, \\ D_{\text{KL}}(p(y|\mathcal{Y}_c) \parallel p(y|x, \mathcal{Y}_c)) &\leq \varepsilon_2, \end{aligned}$$

for all $x \in \text{supp } p(x)$, all $c \in [K]$ and for some non-negative constants $\varepsilon_1, \varepsilon_2 \geq 0$. Assume that the uniform approximation error of the optimization problem $\arg \min_g \mathcal{L}_{\text{NCE}}(g)$ is bounded by a constant $\Delta \geq 0$, i.e., $|g(x, y) - g^*(x, y)| \leq \Delta$ for all $x \in \text{supp } p(x)$ and all $y \in \text{supp } p(y)$. Then, it holds that

$$\min_{W \in \mathbb{R}^{d \times K}, b \in \mathbb{R}^K} \mathcal{L}_{\text{sup}}(W^\top f_{\mathcal{X}}(\cdot) + b) - \mathcal{L}_{\text{sup}}(h^*) \leq \varepsilon_1 + \varepsilon_2 + 2\Delta. \quad (11)$$

5 AUGMENTED SIMILARITY BY NONLINEAR KERNEL AND KERNEL MEAN EMBEDDING

In the previous section, we have observed that the optimal similarity in the pretraining is achieved by the pointwise mutual information and that it makes the class of linear classifiers on the obtained representation contain the optimal classifier. Here, a question arises: “To what extent can the class of similarity approximate the pointwise mutual information?” In Section 5.1, we show a limitation of bilinear similarity that is commonly used in CLIP models. In Section 5.2, we propose a new class of similarities that measures the similarity between two sets of points with a nonlinear kernel. In Section 5.3, we show a potential benefit of using the similarity between two sets of points in terms of the approximation capability of the class.

5.1 LIMITATION OF THE BILINEAR SIMILARITY

Consider d -dimensional feature space. We assume that there are $M (> d + 1)$ pairs of samples, $(x_1, y_1), \dots, (x_M, y_M) \in \mathcal{X} \times \mathcal{Y}$. We define $Z_{\mathcal{X}} \in \mathbb{R}^{d \times M}$ as the concatenation of all features of x_1, \dots, x_M , $Z_{\mathcal{X}} := [f_{\mathcal{X}}(x_1), \dots, f_{\mathcal{X}}(x_M)]$. Similarly, we define $Z_{\mathcal{Y}} \in \mathbb{R}^{d \times M}$ as $Z_{\mathcal{Y}} := [f_{\mathcal{Y}}(y_1), \dots, f_{\mathcal{Y}}(y_M)]$. During pretraining with the symmetric InfoNCE, for some constant $C \in \mathbb{R}$, $Z_{\mathcal{X}}^{\top} Z_{\mathcal{Y}} - C J$ is fit to $G \in \mathbb{R}^{M \times M}$, where $G_{ij} = \ln \frac{p(x_i, y_j)}{p(x_i)p(y_j)}$ and $J \in \mathbb{R}^{M \times M}$ is the matrix of which all items are 1. About the approximation error of the pointwise mutual information, it holds that $\sup_{x \in \text{supp } p(x), y \in \text{supp } p(y)} |g(x, y) - g^*(x, y)| \geq \sup_{i, j} |(Z_{\mathcal{X}}^{\top} Z_{\mathcal{Y}})_{ij} - C - G_{ij}|$. However, it holds that $\text{rank}(Z_{\mathcal{X}}^{\top} Z_{\mathcal{Y}} + C J) \leq d + 1$ (See Proposition C.1). Thus, if the rank of G is $M > d + 1$, there exists a certain error of the approximation of G . In other words, to completely capture the structure of the pointwise mutual information with the bilinear similarity, the dimension of feature d is required to be more than the number of intrinsic instances in the data space, which should be infeasible in the real-world case.

5.2 PROPOSED METHOD: AUGMENTED SIMILARITY BY A NONLINEAR KERNEL AND THE KERNEL MEAN EMBEDDING

Increasing the dimension of the feature is the simplest way to enhance the capability of the similarity. However, this often requires a larger deep neural network model, which leads to heavier computation both in the contrastive learning phase and in downstream tasks. Unlike this approach, we propose to enrich the class of similarity by using a nonlinear kernel function and sets of points. Figure 1 shows the overview of the proposed method. In our approach, we replace the similarity in the symmetric InfoNCE with a similarity between two sets of points produced by encoders. Note that this design is applicable to other modalities although we focus on text-image representation for the sake of simplicity.

Following CLIP, we use two encoders that transform an input from each modality: the image encoder and the text encoder. Instead of a point in the latent space \mathbb{R}^d , the encoders are modified to produce a set of points in the latent space $\{v_i\}_{i \in [M]}$ where $v_i \in \mathbb{R}^d$ for each i . There are choices of model architectures to produce a set of points from an image or a text. Here, we propose to utilize the structure of transformers (Figure 2). We model the encoders with a Vision Transformer (Dosovitskiy et al., 2020) and a Transformer (Vaswani et al., 2017). A general Vision Transformer takes projected patches of an image and the special token, [CLS], and repeats the transformation of vectors with the attention mechanism. As the embedding, it outputs the resulting vector at the position of [CLS] token. On the other hand, our vision encoder outputs whole resulted vectors as the representation. In the same way, we modify the transformer for texts to outputs whole resulting vectors instead of the vector at the position of the special token, [EOS]. In this way, we can modify encoders to produce a set of points without any significant change in the size of the models.

Next, we explain how to calculate the similarity of two sets of points. Given a kernel function $k(\cdot, \cdot): \mathbb{R}^d \times \mathbb{R}^d \rightarrow \mathbb{R}$, we can regard $k(u, v)$ as the similarity between two points u and v . This notion of similarity can be extended to the similarity between two sets of points by the kernel mean embedding (Smola et al., 2007) of Dirac measures (Muandet et al., 2017). Given a kernel k , we

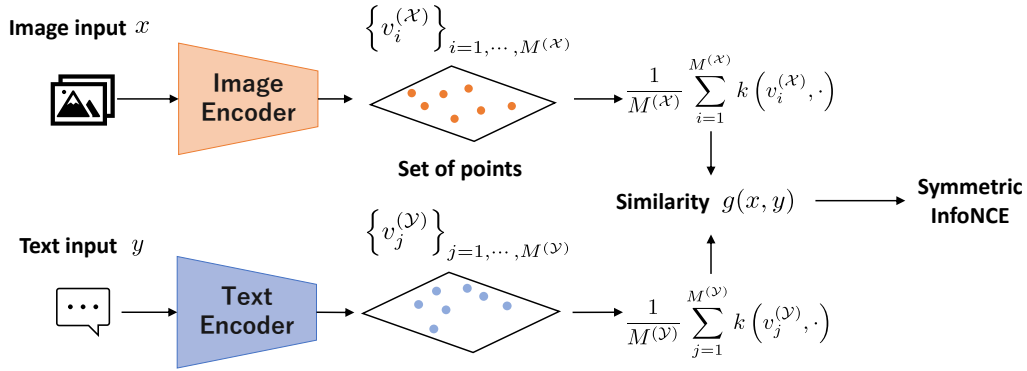


Figure 1: Overview of the proposed method. Each encoder produces a set of points from an input. Similarity between two sets of points is calculated by Eq. 12. The similarity can be regarded as the inner product of the kernel mean embeddings (Smola et al., 2007) of the linear combination of Dirac measures associated with the sets of points. The encoders are optimized with the Symmetric InfoNCE with the similarity matrix.

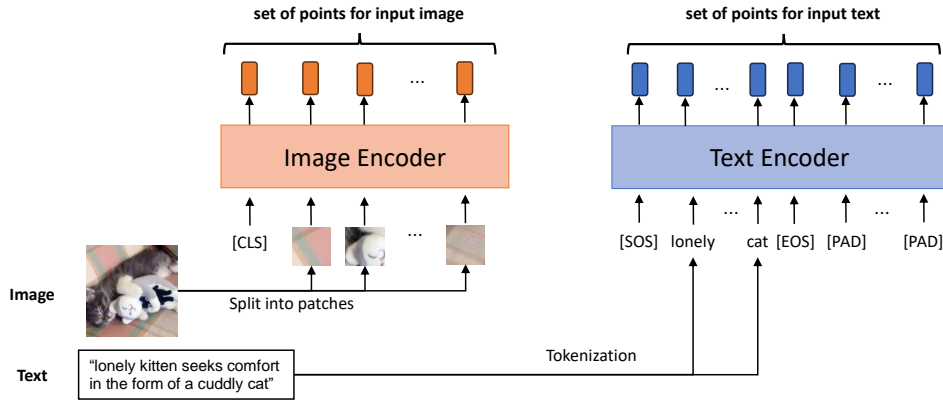


Figure 2: An example of modification for encoders to produce a set of points. Encoders are modeled by Transformer. The encoders output the whole resulted vectors instead of a vector at a certain position.

define the similarity of two sets of points as follows:

$$\begin{aligned} \tilde{g}\left(\left\{v_i^{(\mathcal{X})}\right\}_{i \in [M^{(\mathcal{X})}]}, \left\{v_j^{(\mathcal{Y})}\right\}_{j \in [M^{(\mathcal{Y})}]}\right) &:= \frac{1}{M^{(\mathcal{X})}M^{(\mathcal{Y})}} \sum_{i,j} k(v_i^{(\mathcal{X})}, v_j^{(\mathcal{Y})}) & (12) \\ &= \left\langle \frac{1}{M^{(\mathcal{X})}} \sum_{i=1}^{M^{(\mathcal{X})}} k(v_i^{(\mathcal{X})}, \cdot), \frac{1}{M^{(\mathcal{Y})}} \sum_{j=1}^{M^{(\mathcal{Y})}} k(v_j^{(\mathcal{Y})}, \cdot) \right\rangle_{\mathcal{H}} & (13) \end{aligned}$$

Here, $\langle \cdot, \cdot \rangle_{\mathcal{H}}$ denotes the inner product of the reproducing kernel Hilbert space associated with k . We propose to use this similarity in the symmetric InfoNCE after we scale it by the inverse temperature $1/\tau$. We also propose to use the kernel mean embedding $\frac{1}{M} \sum_{i=1}^M k(v_i, \cdot)$ as the embedding of an input like an image and a text.

Algorithm 1 Symmetric InfoNCE with the similarity between sets of points

Input: vision encoder $f_{\mathcal{X}}$, text encoder $f_{\mathcal{Y}}$, aligned images and texts $\{(x_b, y_b)\}_{b=1}^B$, distribution p associated with the Fourier transform of the shift-invariant kernel \tilde{k} , coefficients α_1 and α_2 , temperature τ .

$$\{v_{b1}^{(\mathcal{X})}, \dots, v_{bM^{(\mathcal{X})}}^{(\mathcal{X})}\} \leftarrow f_{\mathcal{X}}(x_b) \text{ for each } b = 1, \dots, B.$$

$$\{v_{b1}^{(\mathcal{Y})}, \dots, v_{bM^{(\mathcal{Y})}}^{(\mathcal{Y})}\} \leftarrow f_{\mathcal{Y}}(y_b) \text{ for each } b = 1, \dots, B.$$

$$\bar{v}_b^{(\mathcal{X})} \leftarrow \frac{1}{M^{(\mathcal{X})}} \sum_{i=1}^{M^{(\mathcal{X})}} v_{bi}^{(\mathcal{X})}$$

$$\bar{v}_b^{(\mathcal{Y})} \leftarrow \frac{1}{M^{(\mathcal{Y})}} \sum_{j=1}^{M^{(\mathcal{Y})}} v_{bj}^{(\mathcal{Y})}$$

Draw D i.i.d. samples $\omega_1, \dots, \omega_D$ from p .

Draw D i.i.d. samples β_1, \dots, β_D from $\text{Unif}[0, 2\pi)$.

$$z_b^{(\mathcal{X})} \leftarrow \frac{1}{M^{(\mathcal{X})}} \sum_{i=1}^{M^{(\mathcal{X})}} z(v_{bi}^{(\mathcal{X})}; \{\omega_t\}_{t=1}^D, \{\beta_t\}_{t=1}^D)$$

$$z_b^{(\mathcal{Y})} \leftarrow \frac{1}{M^{(\mathcal{Y})}} \sum_{j=1}^{M^{(\mathcal{Y})}} z(v_{bj}^{(\mathcal{Y})}; \{\omega_t\}_{t=1}^D, \{\beta_t\}_{t=1}^D)$$

$$s_{bb'} \leftarrow \tau^{-1} \left(\alpha_1 \bar{v}_b^{(\mathcal{X})\top} \bar{v}_{b'}^{(\mathcal{Y})} + \alpha_2 z_b^{(\mathcal{X})\top} z_{b'}^{(\mathcal{Y})} \right)$$

Compute symmetric InfoNCE from the similarity matrix $\{s_{bb'}\}_{bb'}$.

As the choice of the kernel function, we use the following weighted combination of the linear kernel and a nonlinear kernel \tilde{k} with coefficients $\alpha_1, \alpha_2 \in \mathbb{R}_{\geq 0}$:

$$k(u, v) = \alpha_1 u^\top v + \alpha_2 \tilde{k}(u, v). \quad (14)$$

Here, we also use a trick for faster implementation. In fact, the computation of the similarity in Eq. 12 cannot be performed by a simple matrix multiplication that can be done quickly with GPU. Also, the dimension of the kernel mean embedding in Eq. 13 is basically infinite. To solve these problems for implementation, we use random Fourier features (RFF) (Rahimi & Recht, 2007). When the kernel \tilde{k} is shift-invariant, RFF approximates the kernel $\tilde{k}(u, v)$ by the inner product of two D -dimensional vectors, i.e. $z(u)^\top z(v) \approx \tilde{k}(u, v)$. $z(v) \in \mathbb{R}^D$ is constructed stochastically as follows:

$$z(v; \{\omega_t\}_{t=1}^D, \{\beta_t\}_{t=1}^D) = \sqrt{\frac{1}{2D}} [\cos(\omega_1^\top v + \beta_1), \dots, \cos(\omega_D^\top v + \beta_D)]^\top,$$

where $\omega_t \in \mathbb{R}^M$ and $\beta_t \in \mathbb{R}$ ($t = 1, \dots, D$) are independently sampled from a certain distribution dependent on the kernel \tilde{k} . By taking the average of RFFs obtained from points in the set, we get an embedding of the set of points. More rigorously, this can be regarded as the kernel mean embedding of probability measures where the RFF approximation is applied to obtain finite dimensional representations of the embeddings. For the linear kernel, the similarity of two sets of points is equal to the usual inner product between the average vectors.

$$\frac{1}{M^{(\mathcal{X})}M^{(\mathcal{Y})}} \sum_{i,j} v_i^{(\mathcal{X})\top} v_j^{(\mathcal{Y})} = \left(\frac{1}{M^{(\mathcal{X})}} \sum_{i=1}^{M^{(\mathcal{X})}} v_i^{(\mathcal{X})} \right)^\top \left(\frac{1}{M^{(\mathcal{Y})}} \sum_{j=1}^{M^{(\mathcal{Y})}} v_j^{(\mathcal{Y})} \right).$$

In the implementation, we use the concatenation of the random Fourier feature and the averaged feature as the embedding vector. Overall, Algorithm 1 shows a pseudocode of the proposed loss.

5.3 ON CAPABILITY OF SIMILARITY BASED ON NONLINEAR KERNEL AND SETS OF POINTS

In this section, we show a result regarding the capability of the similarity between two sets of points. Here, we consider a broader class of similarities between two sets of points than Eq. 13, by allowing each point $v_i^{(\mathcal{X})}, v_j^{(\mathcal{Y})} \in \mathbb{R}^d$ to have a weight $w_i^{(\mathcal{X})}, w_j^{(\mathcal{Y})} \in \mathbb{R}$, respectively:

$$\begin{aligned}
& \tilde{g} \left(\left\{ \left(w_i^{(\mathcal{X})}, v_i^{(\mathcal{X})} \right) \right\}_{i \in [M^{(\mathcal{X})}]}, \left\{ \left(w_j^{(\mathcal{Y})}, v_j^{(\mathcal{Y})} \right) \right\}_{j \in [M^{(\mathcal{Y})}]} \right) \\
& := \sum_{i,j} w_i^{(\mathcal{X})} w_j^{(\mathcal{Y})} k(v_i^{(\mathcal{X})}, v_j^{(\mathcal{Y})}) \\
& = \left\langle \sum_{i=1}^{M^{(\mathcal{X})}} w_i^{(\mathcal{X})} k(v_i^{(\mathcal{X})}, \cdot), \sum_{j=1}^{M^{(\mathcal{Y})}} w_j^{(\mathcal{Y})} k(v_j^{(\mathcal{Y})}, \cdot) \right\rangle_{\mathcal{H}}. \tag{15}
\end{aligned}$$

When we set $w_i^{(\mathcal{X})} = 1/M^{(\mathcal{X})}$ for every $i \in [M^{(\mathcal{X})}]$ and $w_j^{(\mathcal{Y})} = 1/M^{(\mathcal{Y})}$ for every $j \in [M^{(\mathcal{Y})}]$, Eq. 15 is equal to Eq. 13. Regarding the capability of this similarity, we have the following result.

Theorem 5.1. *Assume that Assumption C.2 holds. Define a function \tilde{g} as Eq. 15 with a bounded c_0 -universal kernel $k: \mathbb{R}^d \times \mathbb{R}^d \rightarrow \mathbb{R}$. Then, for any $\varepsilon > 0$, there exist positive integers, $M^{(\mathcal{X})}, M^{(\mathcal{Y})} \in \mathbb{N}$ and maps, $f_{\mathcal{X}}: x \mapsto \left\{ \left(w_i^{(\mathcal{X})}, v_i^{(\mathcal{X})} \right) \right\}_{i \in [M^{(\mathcal{X})}]}$ and $f_{\mathcal{Y}}: y \mapsto \left\{ \left(w_j^{(\mathcal{Y})}, v_j^{(\mathcal{Y})} \right) \right\}_{j \in [M^{(\mathcal{Y})}]}$ such that*

$$\sup_{x \in \text{supp } p(x), y \in \text{supp } p(y)} \left| \tilde{g}(f_{\mathcal{X}}(x), f_{\mathcal{Y}}(y)) - \ln \frac{p(x, y)}{p(x)p(y)} \right| < \varepsilon. \tag{16}$$

The proof and Assumption C.2 are provided in Section C.2. For the definition of c_0 -universal kernel, please refer to Sriperumbudur et al. (2011) or see Definition C.5. For example, the Gaussian kernel and the inverse multiquadratic (IMQ) kernel are c_0 -universal (Sriperumbudur et al., 2011).

Unlike the class of the bilinear similarity in Section 5.1, Assumption C.2 doesn't require the dimension d proportional to the number of intrinsic instances. Instead, this requires d larger than or equal to the intrinsic dimensions of subspaces of $x \in \mathcal{X}$ and $y \in \mathcal{Y}$ that have the dependency on each other. However, we claim that this assumption on d is fairly mild because *the manifold hypothesis* (Bengio et al., 2013) is commonly assumed. Although increasing $M^{(\mathcal{X})}$ and $M^{(\mathcal{Y})}$ also leads to heavy computation, at least it provides a different approach to augment representation models from just increasing the feature dimensions.

Lastly, we repeat that this class of the similarity in Eq. 15 is broader than the class we explained in Section 5.2. We leave the investigation of model architectures that provide this class of similarity as future work.

6 EXPERIMENTS

6.1 PRETRAINING

To examine the proposed similarity and the encoders in Section 5.2, we conducted experiments of training a text-image representation model. As the base architecture of the image encoder, we adopted ViT-B/16 (Dosovitskiy et al., 2020). Following the setting of SLIP (Mu et al., 2022), we used the smallest text Transformer model from CLIP, which was a 12-layer 512-wide transformer with 8 attention heads. We used a byte pair encoding (BPE) tokenizer with a vocabulary size of 49K and a maximum context length of 77.

We modified the image encoder and the text encoder to produce sets of points, $v_i^{(\mathcal{X})}$ ($i \in [M^{(\mathcal{X})}]$) and $v_j^{(\mathcal{Y})}$ ($j \in [M^{(\mathcal{Y})}]$), in the way explained in Section 5.2. In addition, we modified the special tokens for padding, [PAD] in Figure 2, for the text encoder to be dependent on its position in order to avoid repeating same tokens. From the settings of encoders, $M^{(\mathcal{X})}$, $M^{(\mathcal{Y})}$ and d were set to 197, 77 and 512, respectively. All vectors in the sets were L2-normalized before the computation of the similarity in Eq. 12. As a nonlinear kernel in Eq. 14, we chose the Gaussian kernel $\tilde{k}(u, v) = \exp\left(-\frac{1}{2\sigma^2}\|u - v\|_2^2\right)$ and the inverse multiquadratic (IMQ) kernel $\tilde{k}(u, v) = \frac{c}{\sqrt{c^2 + \|u - v\|_2^2}}$. After hyperparameter searching, we used $\sigma = 0.3$ for the Gaussian kernel, and $c = 0.5$ for the IMQ kernel. On CC3M, we used both the Gaussian kernel and the IMQ kernel. On 12M, we used only the Gaussian kernel. For the choice of (α_1, α_2) in Eq. 14, we used (0.75, 0.25), (0.5, 0.5) and (0.25, 0.75). During the pretraining, we

Table 1: Zero-shot top-1 classification accuracy (%). Models were trained on CC3M. The gray background indicates the models based on the proposed similarity of sets of points.

Model	Average	ImageNet	CIFAR-10	CIFAR-100	MNIST	STL-10	Food-101	Caltech-101	Cars	SUN397
CLIP	32.70	17.42	49.05	24.04	13.94	83.19	11.79	60.79	0.82	33.28
cossim \circ mean	30.61	18.44	39.79	21.78	10.40	78.49	10.40	60.87	1.03	34.26
Gaussian (75, 25)	32.65	18.59	48.74	23.93	8.92	81.62	13.61	62.08	1.15	35.20
Gaussian (50, 50)	33.54	19.05	55.68	27.21	10.59	81.93	12.93	60.32	1.19	32.94
Gaussian (25, 75)	33.45	20.46	47.50	24.59	15.25	80.26	12.38	63.62	0.98	35.99
IMQ (75, 25)	31.89	18.19	48.87	22.48	9.74	79.82	12.41	60.56	1.23	33.70
IMQ (50, 50)	32.12	18.79	49.57	22.99	10.19	79.98	12.12	61.16	1.17	33.10
IMQ (25, 75)	33.35	18.93	53.69	24.86	11.38	81.60	11.50	62.81	1.04	34.32

Table 2: Zero-shot top-1 classification accuracy (%). Models were trained on CC12M. The gray background indicates the models based on the proposed similarity of sets of points.

Model	Average	ImageNet	CIFAR-10	CIFAR-100	MNIST	STL-10	Food-101	Caltech-101	Cars	SUN397
CLIP	43.16	33.86	57.81	28.02	11.32	86.45	38.74	70.63	19.10	42.54
cossim \circ mean	46.73	36.42	58.39	32.09	21.01	87.96	45.80	71.16	22.06	45.68
Gaussian (75, 25)	47.04	36.22	68.47	32.72	10.08	89.38	45.64	72.85	20.79	47.18
Gaussian (50, 50)	45.87	36.63	60.25	29.89	10.90	89.35	46.12	74.96	19.12	45.59
Gaussian (25, 75)	44.49	35.61	57.25	29.01	6.90	90.56	43.07	72.55	18.81	46.67

set the dimension D of RFFs to 512. For each batch, new ω_t and β_t for RFFs were sampled during the pretraining. We denote pretrained models by the used kernel and $(100\alpha_1, 100\alpha_2)$, e.g., Gaussian (75, 25). For comparison, we also trained our CLIP baseline. Moreover, to ablate the modification of encoders, we trained a model that produces sets of points but was optimized using the cosine similarity of average vectors in the sets. We denote this model as ‘‘cossim \circ mean’’.

For pretraining, We used Conceptual Captions 3M (CC3M) (Sharma et al., 2018) and Conceptual Captions 12M (CC12M) (Changpinyo et al., 2021). As a data augmentation, images were randomly resized and cropped with a scaling factor between 0.5 and 1.0. On CC3M, models were trained for 64 epochs with a batch size of 384. On CC12M, models were trained for 35 epochs with a batch size of 4096. We used the AdamW optimizer with a beta2 of 0.98 and cosine scheduling with a linear warmup in pretraining. We set the initial learning rate to 0.0005. We used weight decay of 0.2 and 0.5 on CC3M and CC12M, respectively. We used the built-in automatic mixed precision library in Pytorch (Paszke et al., 2019). To stabilize the pretraining, we used BF16 on CC12M. We used FP16 on CC3M.

6.2 ZERO-SHOT TRANSFER

We evaluated the zero-shot classification on the following nine benchmark datasets: ImageNet (Russakovsky et al., 2015), CIFAR-10 (Krizhevsky, 2009), CIFAR-100 (Krizhevsky, 2009), MNIST (LeCun et al., 1998), STL-10 (Coates et al., 2011), Food-101 (Bossard et al., 2014), Caltech-101 (Fei-Fei et al., 2006), Stanford Cars (Krause et al., 2013) and SUN397 (Xiao et al., 2010). Following SLIP (Mu et al., 2022), we adopted prompt ensembling. Prompts provided by SLIP for each dataset were used. We set the dimension D of RFFs to 512. ω_t and β_t for RFFs were fixed before the evaluation. To see the effect of the randomness of RFFs, we performed five zero-shot evaluations for models that use a nonlinear kernel.

Table 3: Top-1 accuracy of linear classification tasks (%). Models were trained on CC3M.

Model	Average	CIFAR-10	CIFAR-100	MNIST	STL-10	Food-101	Caltech-101	Cars	SUN397
CLIP before projection	72.59	84.09	62.94	94.49	91.51	62.15	81.54	37.20	66.78
CLIP	64.34	77.21	49.2	89.10	90.21	48.17	81.05	19.67	60.10
cossim \circ mean	62.17	74.5	45.17	88.55	90.86	47.30	80.49	16.76	53.70
Gaussian (50, 50)	65.75	78.82	52.48	89.73	91.36	50.42	82.14	19.69	61.39

Table 4: Top-1 accuracy of linear classification evaluation (%). Models were trained on CC12M.

Model	Average	CIFAR-10	CIFAR-100	MNIST	STL-10	Food-101	Caltech-101	Cars	SUN397
CLIP before projection	82.02	88.43	68.38	96.52	95.33	77.41	87.48	67.96	74.68
CLIP	77.15	83.42	58.16	93.53	94.89	72.43	87.23	57.98	69.56
cossim \circ mean	75.87	80.92	53.86	92.89	95.34	72.95	87.86	58.08	65.05
Gaussian (75, 25)	77.60	84.24	57.79	91.45	95.61	73.54	88.07	59.08	71.00

Table 1 and 2 show the result of zero-shot classifications. Results of models using RFFs have been averaged. In Table 5 and 6, we also shows the standard deviation. We find that the proposed method outperformed the CLIP on average with proper hyperparameter settings. From the comparison to the cossim \circ mean, we also find that the proposed similarity computed by using sets of points and a nonlinear kernel were beneficial to average performance. In addition, we find that the randomness of RFFs did not have a significant impact on the overall performance.

6.3 LINEAR CLASSIFICATION

We also performed the linear classification evaluation where we trained linear classifiers on the embedding vector obtained by frozen pretrained image encoders. We used eight benchmark datasets: CIFAR-10, CIFAR-100, MNIST, STL-10, Caltech-101, Stanford Cars and SUN397. Based on the result of zero-shot classification, we used the Gaussian (50, 50) model trained on CC3M, and the Gaussian (75, 25) model trained on CC12M. We set D for RFFs to 256. ω_t and β_t were fixed before the evaluation. Based on the robustness of RFFs shown in Table 5 and 6, we didn't evaluate multiple settings of ω_t and β_t for the linear classifications. For comparison, we also used our CLIPs and cossim \circ mean models. We trained linear classifiers on the embeddings that were used for computation of the similarity in the symmetric InfoNCE. Please note that this is a bit different from a common practice, where the intermediate latent vector just before the final projection layer of the image encoder is used as the feature for linear classifiers (Chen et al., 2021). For comparison, we also trained linear classifiers in that manner, which we denote as "CLIP before projection".

We used Momentum SGD with a momentum of 0.9 and cosine scheduling. We used no weight decay. Linear classifiers were trained for 90 epochs. On datasets that have less than 10000 training images, i.e., Stanford Cars, STL-10 and Caltech-101, we set the initial learning rate to 0.05 and used a batch size of 1024. On the other datasets, i.e., CIFAR-10, CIFAR-100, Food-101, MNIST and SUN397, we set the initial learning rate to 0.01 and used a batch size of 4096.

Table 3 and 4 show the results of linear classification evaluations. We find that the proposed embedding outperformed the CLIP and the cossim \circ mean on most of the datasets. The results suggest that the proposed similarity computed with sets of points and a nonlinear kernel helps to obtain multimodal representation on a shared space. However, we also find that the performance of

linear image classifications was worse than the results with the intermediate latent vectors. We leave filling this gap in performance empirically and theoretically as future work.

7 CONCLUSIONS AND FUTURE WORK

We presented a new understanding of the symmetric InfoNCE through the lens of the pointwise mutual information. We spotlighted that the optimal similarity of the symmetric InfoNCE is represented by the pointwise mutual information. We showed that we can construct a linear classifier close to the optimal classifier of downstream tasks that is possibly nonlinear when the optimal similarity is obtained. We also showed the effect on the performance of downstream tasks caused by the deviation of the obtained similarity from the pointwise mutual information. Based on this theoretical result, we proposed a new class of similarities for contrastive learning to reduce the deviation from the pointwise mutual information. With this class, the similarity of two sets of points provided by encoders is calculated by a nonlinear kernel. We showed the theoretical rationale for using the similarity of two sets of points with a nonlinear kernel. In experiments on CC3M and CC12M, we demonstrated the performance of the proposed method. We leave the investigation of better model architectures for the similarity of sets of points as future work.

ACKNOWLEDGEMENTS

Computational resource of AI Bridging Cloud Infrastructure (ABCI) provided by National Institute of Advanced Industrial Science and Technology (AIST) was used. TS was partially supported by JSPS KAKENHI (20H00576) and JST CREST (JPMJCR2015).

REFERENCES

- Jean-Baptiste Alayrac, Jeff Donahue, Pauline Luc, Antoine Miech, Iain Barr, Yana Hasson, Karel Lenc, Arthur Mensch, Katherine Millican, Malcolm Reynolds, et al. Flamingo: a visual language model for few-shot learning. *Advances in Neural Information Processing Systems*, 35:23716–23736, 2022.
- Nachman Aronszajn. Theory of reproducing kernels. *Transactions of the American mathematical society*, 68(3):337–404, 1950.
- Jordan Ash, Surbhi Goel, Akshay Krishnamurthy, and Dipendra Misra. Investigating the role of negatives in contrastive representation learning. In *Proceedings of The 25th International Conference on Artificial Intelligence and Statistics*, volume 151, pp. 7187–7209, 28–30 Mar 2022.
- Philip Bachman, R Devon Hjelm, and William Buchwalter. Learning representations by maximizing mutual information across views. In *Advances in Neural Information Processing Systems*, volume 32, 2019.
- Yoshua Bengio, Aaron Courville, and Pascal Vincent. Representation learning: A review and new perspectives. *IEEE transactions on pattern analysis and machine intelligence*, 35(8):1798–1828, 2013.
- Lukas Bossard, Matthieu Guillaumin, and Luc Van Gool. Food-101—mining discriminative components with random forests. In *Computer Vision—ECCV 2014: 13th European Conference, Zurich, Switzerland, September 6–12, 2014, Proceedings, Part VI 13*, pp. 446–461, 2014.
- Soravit Changpinyo, Piyush Sharma, Nan Ding, and Radu Soricut. Conceptual 12m: Pushing web-scale image-text pre-training to recognize long-tail visual concepts. In *Proceedings of the IEEE/CVF Conference on Computer Vision and Pattern Recognition*, pp. 3558–3568, 2021.
- Ting Chen, Simon Kornblith, Mohammad Norouzi, and Geoffrey Hinton. A simple framework for contrastive learning of visual representations. In *International conference on machine learning*, pp. 1597–1607, 2020.
- Xinlei Chen, Saining Xie, and Kaiming He. An empirical study of training self-supervised vision transformers. In *Proceedings of the IEEE/CVF International Conference on Computer Vision (ICCV)*, pp. 9640–9649, October 2021.

-
- Sumit Chopra, Raia Hadsell, and Yann LeCun. Learning a similarity metric discriminatively, with application to face verification. In *2005 IEEE computer society conference on computer vision and pattern recognition (CVPR'05)*, volume 1, pp. 539–546, 2005.
- Adam Coates, Andrew Ng, and Honglak Lee. An analysis of single-layer networks in unsupervised feature learning. In *Proceedings of the fourteenth international conference on artificial intelligence and statistics*, pp. 215–223, 2011.
- Karan Desai, Maximilian Nickel, Tanmay Rajpurohit, Justin Johnson, and Shanmukha Ramakrishna Vedantam. Hyperbolic image-text representations. In *International Conference on Machine Learning*, pp. 7694–7731, 2023.
- Alexey Dosovitskiy, Lucas Beyer, Alexander Kolesnikov, Dirk Weissenborn, Xiaohua Zhai, Thomas Unterthiner, Mostafa Dehghani, Matthias Minderer, Georg Heigold, Sylvain Gelly, et al. An image is worth 16x16 words: Transformers for image recognition at scale. *arXiv preprint arXiv:2010.11929*, 2020.
- Benjamin Elizalde, Soham Deshmukh, Mahmoud Al Ismail, and Huaming Wang. Clap learning audio concepts from natural language supervision. In *ICASSP 2023-2023 IEEE International Conference on Acoustics, Speech and Signal Processing (ICASSP)*, pp. 1–5, 2023.
- Li Fei-Fei, Robert Fergus, and Pietro Perona. One-shot learning of object categories. *IEEE transactions on pattern analysis and machine intelligence*, 28(4):594–611, 2006.
- Andreas Furst, Elisabeth Rumetshofer, Johannes Lehner, Viet T. Tran, Fei Tang, Hubert Ramsauer, David Kreil, Michael Kopp, Gnter Klambauer, Angela Bitto, and Sepp Hochreiter. Cloob: Modern hopfield networks with infoloob outperform clip. In *Advances in Neural Information Processing Systems*, volume 35, pp. 20450–20468, 2022.
- Rohit Girdhar, Alaaeldin El-Nouby, Zhuang Liu, Mannat Singh, Kalyan Vasudev Alwala, Armand Joulin, and Ishan Misra. Imagebind: One embedding space to bind them all. In *Proceedings of the IEEE/CVF Conference on Computer Vision and Pattern Recognition*, pp. 15180–15190, 2023.
- Shashank Goel, Hritik Bansal, Sumit Bhatia, Ryan Rossi, Vishwa Vinay, and Aditya Grover. Cyclip: Cyclic contrastive language-image pretraining. *Advances in Neural Information Processing Systems*, 35:6704–6719, 2022.
- Wenzhong Guo, Jianwen Wang, and Shiping Wang. Deep multimodal representation learning: A survey. *Ieee Access*, 7:63373–63394, 2019.
- Andrey Guzhov, Federico Raue, Jrn Hees, and Andreas Dengel. Audioclip: Extending clip to image, text and audio. In *ICASSP 2022-2022 IEEE International Conference on Acoustics, Speech and Signal Processing (ICASSP)*, pp. 976–980, 2022.
- Jeff Z HaoChen, Colin Wei, Adrien Gaidon, and Tengyu Ma. Provable guarantees for self-supervised deep learning with spectral contrastive loss. *Advances in Neural Information Processing Systems*, 34:5000–5011, 2021.
- R Devon Hjelm, Alex Fedorov, Samuel Lavoie-Marchildon, Karan Grewal, Phil Bachman, Adam Trischler, and Yoshua Bengio. Learning deep representations by mutual information estimation and maximization. In *International Conference on Learning Representations*, 2019.
- Weiran Huang, Mingyang Yi, Xuyang Zhao, and Zihao Jiang. Towards the generalization of contrastive self-supervised learning. In *The Eleventh International Conference on Learning Representations*, 2023.
- Chao Jia, Yinfei Yang, Ye Xia, Yi-Ting Chen, Zarana Parekh, Hieu Pham, Quoc Le, Yun-Hsuan Sung, Zhen Li, and Tom Duerig. Scaling up visual and vision-language representation learning with noisy text supervision. In *International conference on machine learning*, pp. 4904–4916, 2021.
- Jonathan Krause, Michael Stark, Jia Deng, and Li Fei-Fei. 3d object representations for fine-grained categorization. In *Proceedings of the IEEE international conference on computer vision workshops*, pp. 554–561, 2013.

-
- Alex Krizhevsky. Learning multiple layers of features from tiny images. 2009.
- Yann LeCun, Léon Bottou, Yoshua Bengio, and Patrick Haffner. Gradient-based learning applied to document recognition. *Proceedings of the IEEE*, 86(11):2278–2324, 1998.
- Junnan Li, Ramprasaath Selvaraju, Akhilesh Gotmare, Shafiq Joty, Caiming Xiong, and Steven Chu Hong Hoi. Align before fuse: Vision and language representation learning with momentum distillation. *Advances in neural information processing systems*, 34:9694–9705, 2021a.
- Junnan Li, Dongxu Li, Caiming Xiong, and Steven Hoi. Blip: Bootstrapping language-image pre-training for unified vision-language understanding and generation. In *International Conference on Machine Learning*, pp. 12888–12900, 2022.
- Yazhe Li, Roman Pogodin, Danica J Sutherland, and Arthur Gretton. Self-supervised learning with kernel dependence maximization. *Advances in Neural Information Processing Systems*, 34: 15543–15556, 2021b.
- Yan-Bo Lin, Jie Lei, Mohit Bansal, and Gedas Bertasius. Eclipse: Efficient long-range video retrieval using sight and sound. In *European Conference on Computer Vision*, pp. 413–430, 2022.
- Norman Mu, Alexander Kirillov, David Wagner, and Saining Xie. Slip: Self-supervision meets language-image pre-training. In *European Conference on Computer Vision*, pp. 529–544, 2022.
- Krikamol Muandet, Kenji Fukumizu, Bharath Sriperumbudur, Bernhard Schölkopf, et al. Kernel mean embedding of distributions: A review and beyond. *Foundations and Trends® in Machine Learning*, 10(1-2):1–141, 2017.
- Aaron van den Oord, Yazhe Li, and Oriol Vinyals. Representation learning with contrastive predictive coding. *arXiv preprint arXiv:1807.03748*, 2018.
- Adam Paszke, Sam Gross, Francisco Massa, Adam Lerer, James Bradbury, Gregory Chanan, Trevor Killeen, Zeming Lin, Natalia Gimelshein, Luca Antiga, et al. Pytorch: An imperative style, high-performance deep learning library. *Advances in neural information processing systems*, 32, 2019.
- Or Patashnik, Zongze Wu, Eli Shechtman, Daniel Cohen-Or, and Dani Lischinski. Styleclip: Text-driven manipulation of stylegan imagery. In *Proceedings of the IEEE/CVF International Conference on Computer Vision*, pp. 2085–2094, 2021.
- Alec Radford, Jong Wook Kim, Chris Hallacy, Aditya Ramesh, Gabriel Goh, Sandhini Agarwal, Girish Sastry, Amanda Askell, Pamela Mishkin, Jack Clark, et al. Learning transferable visual models from natural language supervision. In *International conference on machine learning*, pp. 8748–8763, 2021.
- Ali Rahimi and Benjamin Recht. Random features for large-scale kernel machines. *Advances in neural information processing systems*, 20, 2007.
- Aditya Ramesh, Prafulla Dhariwal, Alex Nichol, Casey Chu, and Mark Chen. Hierarchical text-conditional image generation with clip latents. *arXiv preprint arXiv:2204.06125*, 1(2):3, 2022.
- Olga Russakovsky, Jia Deng, Hao Su, Jonathan Krause, Sanjeev Satheesh, Sean Ma, Zhiheng Huang, Andrej Karpathy, Aditya Khosla, Michael Bernstein, et al. Imagenet large scale visual recognition challenge. *International journal of computer vision*, 115:211–252, 2015.
- Nikunj Saunshi, Orestis Plevrakis, Sanjeev Arora, Mikhail Khodak, and Hrishikesh Khandeparkar. A theoretical analysis of contrastive unsupervised representation learning. In *Proceedings of the 36th International Conference on Machine Learning*, volume 97, pp. 5628–5637, 09–15 Jun 2019.
- Piyush Sharma, Nan Ding, Sebastian Goodman, and Radu Soricut. Conceptual captions: A cleaned, hypernymed, image alt-text dataset for automatic image captioning. In *Proceedings of the 56th Annual Meeting of the Association for Computational Linguistics (Volume 1: Long Papers)*, pp. 2556–2565, July 2018.

-
- Zhenmei Shi, Jiefeng Chen, Kunyang Li, Jayaram Raghuram, Xi Wu, Yingyu Liang, and Somesh Jha. The trade-off between universality and label efficiency of representations from contrastive learning. In *The Eleventh International Conference on Learning Representations*, 2023.
- Alex Smola, Arthur Gretton, Le Song, and Bernhard Schölkopf. A hilbert space embedding for distributions. In *International conference on algorithmic learning theory*, pp. 13–31, 2007.
- Kihyuk Sohn. Improved deep metric learning with multi-class n-pair loss objective. *Advances in neural information processing systems*, 29, 2016.
- Bharath K Sriperumbudur, Kenji Fukumizu, and Gert RG Lanckriet. Universality, characteristic kernels and rkhs embedding of measures. *Journal of Machine Learning Research*, 12(7), 2011.
- Yonglong Tian, Dilip Krishnan, and Phillip Isola. Contrastive multiview coding. In *Computer Vision—ECCV 2020: 16th European Conference, Glasgow, UK, August 23–28, 2020, Proceedings, Part XI 16*, pp. 776–794, 2020.
- Christopher Tosh, Akshay Krishnamurthy, and Daniel Hsu. Contrastive learning, multi-view redundancy, and linear models. In *Proceedings of the 32nd International Conference on Algorithmic Learning Theory*, volume 132, pp. 1179–1206, 16–19 Mar 2021.
- Michael Tschannen, Josip Djolonga, Paul K. Rubenstein, Sylvain Gelly, and Mario Lucic. On mutual information maximization for representation learning. In *International Conference on Learning Representations*, 2020.
- Ashish Vaswani, Noam Shazeer, Niki Parmar, Jakob Uszkoreit, Llion Jones, Aidan N Gomez, Łukasz Kaiser, and Illia Polosukhin. Attention is all you need. *Advances in neural information processing systems*, 30, 2017.
- Hiroki Waida, Yuichiro Wada, Léo Andéol, Takumi Nakagawa, Yuhui Zhang, and Takafumi Kanamori. Towards understanding the mechanism of contrastive learning via similarity structure: A theoretical analysis. In *Machine Learning and Knowledge Discovery in Databases: Research Track*, pp. 709–727. Springer Nature Switzerland, 2023.
- Tongzhou Wang and Phillip Isola. Understanding contrastive representation learning through alignment and uniformity on the hypersphere. In *International Conference on Machine Learning*, pp. 9929–9939, 2020.
- Yifei Wang, Qi Zhang, Yisen Wang, Jiansheng Yang, and Zhouchen Lin. Chaos is a ladder: A new theoretical understanding of contrastive learning via augmentation overlap. In *International Conference on Learning Representations*, 2022.
- Ho-Hsiang Wu, Prem Seetharaman, Kundan Kumar, and Juan Pablo Bello. Wav2clip: Learning robust audio representations from clip. In *ICASSP 2022-2022 IEEE International Conference on Acoustics, Speech and Signal Processing (ICASSP)*, pp. 4563–4567, 2022.
- Jianxiong Xiao, James Hays, Krista A Ehinger, Aude Oliva, and Antonio Torralba. Sun database: Large-scale scene recognition from abbey to zoo. In *2010 IEEE computer society conference on computer vision and pattern recognition*, pp. 3485–3492, 2010.
- Jiahui Yu, Zirui Wang, Vijay Vasudevan, Legg Yeung, Mojtaba Seyedhosseini, and Yonghui Wu. Coca: Contrastive captioners are image-text foundation models. *arXiv preprint arXiv:2205.01917*, 2022.
- Yuhao Zhang, Hang Jiang, Yasuhide Miura, Christopher D. Manning, and Curtis P. Langlotz. Contrastive learning of medical visual representations from paired images and text. In *Proceedings of the 7th Machine Learning for Healthcare Conference*, volume 182, pp. 2–25, 05–06 Aug 2022.
- Yuhui Zhang, Yuichiro Wada, Hiroki Waida, Kaito Goto, Yusaku Hino, and Takafumi Kanamori. Deep clustering with a constraint for topological invariance based on symmetric infonce. *Neural Computation*, 35(7):1288–1339, 2023.
- Roland S. Zimmermann, Yash Sharma, Steffen Schneider, Matthias Bethge, and Wieland Brendel. Contrastive learning inverts the data generating process. In *Proceedings of the 38th International Conference on Machine Learning*, volume 139, pp. 12979–12990, 18–24 Jul 2021.

A ADDITIONAL EMPIRICAL RESULTS

In this section, we shows results of the same zero-shot classification in Section 6.2 but with the standard deviation.

Table 5: Zero-shot top-1 classification accuracy (%). Models were trained on CC3M.

Dataset	Gaussian (75, 25)	Gaussian (50, 50)	Gaussian (25, 75)	IMQ (75, 25)	IMQ (50, 50)	IMQ (25, 75)
ImageNet	18.59 ± 0.03	19.05 ± 0.02	20.46 ± 0.04	18.19 ± 0.02	18.79 ± 0.03	18.93 ± 0.12
CIFAR-10	48.74 ± 0.06	55.68 ± 0.15	47.50 ± 0.14	48.87 ± 0.22	49.57 ± 0.38	53.69 ± 0.26
CIFAR-100	23.93 ± 0.04	27.21 ± 0.05	24.59 ± 0.07	22.48 ± 0.08	22.99 ± 0.07	24.86 ± 0.38
MNIST	8.92 ± 0.00	10.59 ± 0.48	15.25 ± 1.03	9.74 ± 0.00	10.19 ± 0.21	11.38 ± 1.18
STL-10	81.62 ± 0.03	81.93 ± 0.08	80.26 ± 0.04	79.82 ± 0.14	79.98 ± 0.37	81.60 ± 0.80
Food-101	13.61 ± 0.05	12.93 ± 0.07	12.38 ± 0.03	12.41 ± 0.03	12.12 ± 0.14	11.50 ± 0.22
Caltech-101	62.08 ± 0.03	60.32 ± 0.07	63.62 ± 0.02	60.56 ± 0.14	61.16 ± 0.18	62.81 ± 0.24
Cars	1.15 ± 0.02	1.19 ± 0.05	0.98 ± 0.02	1.23 ± 0.02	1.17 ± 0.07	1.04 ± 0.07
SUN397	35.20 ± 0.03	32.94 ± 0.08	35.99 ± 0.04	33.70 ± 0.11	33.10 ± 0.03	34.32 ± 0.31

Table 6: Zero-shot top-1 classification accuracy (%). Models were trained on CC12M.

Dataset	Gaussian (75, 25)	Gaussian (50, 50)	Gaussian (25, 75)
ImageNet	36.22 ± 0.02	36.63 ± 0.01	35.61 ± 0.06
CIFAR-10	68.47 ± 0.03	60.25 ± 0.07	57.25 ± 0.08
CIFAR-100	32.72 ± 0.03	29.89 ± 0.06	29.01 ± 0.12
MNIST	10.08 ± 0.09	10.90 ± 0.07	6.90 ± 0.36
STL-10	89.38 ± 0.02	89.35 ± 0.03	90.56 ± 0.12
Food-101	45.64 ± 0.04	46.12 ± 0.04	43.07 ± 0.21
Caltech-101	72.85 ± 0.02	74.96 ± 0.03	72.55 ± 0.22
Cars	20.79 ± 0.08	19.12 ± 0.06	18.81 ± 0.22
SUN397	47.18 ± 0.01	45.59 ± 0.04	46.67 ± 0.15

B PROOFS OF STATEMENTS IN SECTION 4

B.1 PROOF OF THEOREM 4.2

Proof. From the definition of $\bar{h}^g(x)$, the c -th element of $\bar{h}^{g^*}(x)$ is calculated as follows:

$$\begin{aligned}
 \bar{h}^{g^*}(x)_c &= \left(\mathbb{E}_{p(y|\mathcal{Y}_c)} \left[\frac{1}{\tau^*} f_{\mathcal{Y}^*}^*(y) \right] \right)^\top f_{\mathcal{X}^*}^*(x) + \ln P(\mathcal{Y}_c) \\
 &= \mathbb{E}_{p(y|\mathcal{Y}_c)} \left[\frac{1}{\tau^*} f_{\mathcal{Y}^*}^*(y)^\top f_{\mathcal{X}^*}^*(x) \right] + \ln P(\mathcal{Y}_c) \\
 &= \mathbb{E}_{p(y|\mathcal{Y}_c)} [g^*(x, y)] + \ln P(\mathcal{Y}_c) \\
 &= \mathbb{E}_{p(y|\mathcal{Y}_c)} \left[\ln \frac{p(x, y)}{p(x)p(y)} \right] + \ln P(\mathcal{Y}_c) + C.
 \end{aligned}$$

Since adding a constant to all elements of $h(x)$ doesn't change the supervised loss $\mathcal{L}_{\text{sup}}(h)$, we consider $C = 0$ for the sake of simplicity. The c -th element of $\bar{h}^{g^*}(x)$ is further rearranged as

follows:

$$\begin{aligned}
\bar{h}^{g^*}(x)_c &= \mathbb{E}_{p(y|\mathcal{Y}_c)} \left[\ln \frac{p(x, y)}{p(x)p(y)} \right] + \ln P(\mathcal{Y}_c) \\
&= \mathbb{E}_{p(y|\mathcal{Y}_c)} \left[\ln \frac{p(x, y)p(x)P(\mathcal{Y}_c)}{p(x)p(y)p(x, \mathcal{Y}_c)} + \ln \frac{p(x, \mathcal{Y}_c)}{p(x)P(\mathcal{Y}_c)} \right] + \ln P(\mathcal{Y}_c) \\
&= \mathbb{E}_{p(y|\mathcal{Y}_c)} \left[\ln \frac{p(x, y)/p(x, \mathcal{Y}_c)}{p(y)/P(\mathcal{Y}_c)} \right] + \ln \frac{p(x, \mathcal{Y}_c)}{p(x)} \\
&= \mathbb{E}_{p(y|\mathcal{Y}_c)} \left[\ln \frac{p(y|x, \mathcal{Y}_c)}{p(y|\mathcal{Y}_c)} \right] + \ln P(\mathcal{Y}_c|x) \\
&= \ln P(\mathcal{Y}_c|x) - D_{\text{KL}}(p(y|\mathcal{Y}_c) \| p(y|x, \mathcal{Y}_c)).
\end{aligned}$$

Therefore, we have that

$$\begin{aligned}
\mathcal{L}_{\text{sup}}(\bar{h}^{g^*}) - \mathcal{L}_{\text{sup}}(h^*) &= \mathbb{E}_{p(x, c)} \left[\ln P(c|x) - \bar{h}^{g^*}(x)_c + \ln \left(\sum_i \exp \bar{h}^{g^*}(x)_i \right) \right] \\
&= \mathbb{E}_{p(x, c)} \left[\ln P(c|x) - \ln P(\mathcal{Y}_c|x) + D_{\text{KL}}(p(y|\mathcal{Y}_c) \| p(y|x, \mathcal{Y}_c)) \right. \\
&\quad \left. + \ln \left(\sum_i P(\mathcal{Y}_i|x) \cdot \exp(-D_{\text{KL}}(p(y|\mathcal{Y}_i) \| p(y|x, \mathcal{Y}_i))) \right) \right] \\
&\leq \mathbb{E}_{p(x, c)} \left[\ln P(c|x) - \ln P(\mathcal{Y}_c|x) + D_{\text{KL}}(p(y|\mathcal{Y}_c) \| p(y|x, \mathcal{Y}_c)) + \ln \left(\sum_i P(\mathcal{Y}_i|x) \right) \right] \\
&= \mathbb{E}_{p(x, c)} \left[\ln p(c|x) - \ln p(\mathcal{Y}_c|x) + D_{\text{KL}}(p(y|\mathcal{Y}_c) \| p(y|x, \mathcal{Y}_c)) + \ln P(\tilde{\mathcal{Y}}|x) \right] \\
&= \mathbb{E}_{p(x, c)} \left[\ln \frac{P(c|x)}{P(\mathcal{Y}_c|x)/P(\tilde{\mathcal{Y}}|x)} + D_{\text{KL}}(p(y|\mathcal{Y}_c) \| p(y|x, \mathcal{Y}_c)) \right] \\
&= \mathbb{E}_{p(x)} \left[D_{\text{KL}}(P(c|x) \| P(\mathcal{Y}_c|x, \tilde{\mathcal{Y}})) \right] + \mathbb{E}_{p(x, c)} [D_{\text{KL}}(p(y|\mathcal{Y}_c) \| p(y|x, \mathcal{Y}_c))].
\end{aligned}$$

Here, the inequality holds by the monotonicity of $\ln(\cdot)$, the non-negativity of $P(\mathcal{Y}_i|x)$ and the non-negativity of KL divergence. \square

B.2 PROOF OF LEMMA 4.3

Proof. For every $i \in [K]$, it holds that

$$\begin{aligned}
\left| \bar{h}^g(x)_i - \bar{h}^{g^*}(x)_i \right| &= \left| \mathbb{E}_{p(y|\mathcal{Y}_i)} [g(x, y) - g^*(x, y)] \right| \\
&\leq \left| \mathbb{E}_{p(y|\mathcal{Y}_i)} [\Delta] \right| \\
&= \Delta.
\end{aligned}$$

Let $\varsigma_c(z)$ denote the logarithm of the c -th element of the softmax function, i.e., $\varsigma_c(z) := \ln \frac{e^{z_c}}{\sum_{i=1}^K e^{z_i}}$.

$$\begin{aligned}
\left| \mathcal{L}_{\text{sup}}(\bar{h}^g) - \mathcal{L}_{\text{sup}}(\bar{h}^{g^*}) \right| &= \left| \mathbb{E}_{p(x, c)} \left[-\ln \frac{\exp \bar{h}^g(x)_c}{\sum_{i=1}^K \exp \bar{h}^g(x)_i} + \ln \frac{\exp \bar{h}^{g^*}(x)_c}{\sum_{i=1}^K \exp \bar{h}^{g^*}(x)_i} \right] \right| \\
&\leq \mathbb{E}_{p(x, c)} \left[\left| -\varsigma_c(\bar{h}^g(x)) + \varsigma_c(\bar{h}^{g^*}(x)) \right| \right]. \tag{17}
\end{aligned}$$

$\varsigma_c(z)$ is a differentiable function with respect to z , and the partial derivative is given as follows:

$$\begin{aligned}\frac{\partial \varsigma_c}{\partial z_c} &= 1 - \frac{e^{z_c}}{\sum_{i=1}^K e^{z_i}}, \\ \frac{\partial \varsigma_c}{\partial z_j} &= \frac{-e^{z_j}}{\sum_{i=1}^K e^{z_i}} \quad \text{for } j \neq c.\end{aligned}$$

By the mean value theorem, there exists ξ on the line segment between $\bar{h}^g(x)$ and $\bar{h}^{g^*}(x)$ such that

$$-\varsigma_c(\bar{h}^g(x)) + \varsigma_c(\bar{h}^{g^*}(x)) = \nabla \varsigma_c(\xi)^\top \left(-\bar{h}^g(x) + \bar{h}^{g^*}(x) \right).$$

Therefore, we have

$$\begin{aligned}\mathbb{E}_{p(x,c)} \left[\left| -\varsigma_c(\bar{h}^g(x)) + \varsigma_c(\bar{h}^{g^*}(x)) \right| \right] &= \mathbb{E}_{p(x,c)} \left[\left| \nabla \varsigma_c(\xi)^\top \left(-\bar{h}^g(x) + \bar{h}^{g^*}(x) \right) \right| \right] \\ &\leq \mathbb{E}_{p(x,c)} \left[\left(\sum_{i=1}^K \left| \frac{\partial \varsigma_c}{\partial z_i}(\xi) \right| \right) \left\| \bar{h}^g(x) - \bar{h}^{g^*}(x) \right\|_\infty \right] \\ &\leq \mathbb{E}_{p(x,c)} [2\Delta] \\ &= 2\Delta.\end{aligned}\tag{18}$$

Here, the first inequality holds by Hölder's inequality. At the second inequality, we use

$$\sum_{i=1}^K \left| \frac{\partial \varsigma_c}{\partial z_i}(\xi) \right| = 1 - \frac{e^{\xi_c}}{\sum_{i=1}^K e^{\xi_i}} + \frac{\sum_{i \neq c} e^{\xi_i}}{\sum_{i=1}^K e^{\xi_i}} \leq 2.$$

Combining Eq. 17, 18 finishes the proof. \square

C REGARDING THE REPRESENTATIONAL CAPABILITY OF THE CLASS OF SIMILARITIES

C.1 LIMITATION OF THE BILINEAR SIMILARITY

Proposition C.1. *Let $A, B \in \mathbb{R}^{d \times M}$ and $c \in \mathbb{R}$. Let $J \in \mathbb{R}^{M \times M}$ denote the matrix of which all elements are 1. Then, we have that $\text{rank}(A^\top B - cJ) \leq d + 1$.*

Proof. We define $\tilde{A}, \tilde{B} \in \mathbb{R}^{(d+1) \times M}$ as follows:

$$\tilde{A} = \begin{bmatrix} A \\ -1 & \dots & -1 \end{bmatrix}, \quad \tilde{B} = \begin{bmatrix} B \\ c & \dots & c \end{bmatrix}.$$

Then, we have that $\tilde{A}^\top \tilde{B} = A^\top B - cJ$. Since $\text{rank } \tilde{A} \leq d + 1$ and $\text{rank } \tilde{B} \leq d + 1$, the statement follows. \square

C.2 POTENTIAL ADVANTAGE OF THE SIMILARITY BETWEEN SETS OF POINTS

In this section, we denote (joint) probability density functions of random variables by using their corresponding letters. For example, we denote the joint probability density function of the random variables X, Y and the probability density function of X as $p_{X,Y}$ and p_X , respectively.

We impose the following assumptions on the generation process of random variables $X \in \mathcal{X}$ and $Y \in \mathcal{Y}$.

Assumption C.2 (Generation process). There exist random variables $\tilde{X}, \tilde{Y} \in \mathbb{R}^d$, $Z^{(\mathcal{X})} \in \mathbb{R}^{d_{\mathcal{X}}}$ and $Z^{(\mathcal{Y})} \in \mathbb{R}^{d_{\mathcal{Y}}}$ that satisfy the following conditions.

- (a) $(\tilde{X}, \tilde{Y}), Z^{(\mathcal{X})}$ and $Z^{(\mathcal{Y})}$ are mutually independent.

- (b) There exist continuous bijective mappings $h_{\mathcal{X}}: \mathbb{R}^d \times \mathbb{R}^{d_{\mathcal{X}}} \rightarrow \mathcal{X}$ and $h_{\mathcal{Y}}: \mathbb{R}^d \times \mathbb{R}^{d_{\mathcal{Y}}} \rightarrow \mathcal{Y}$ such that $X = h_{\mathcal{X}}(\tilde{X}, Z^{(\mathcal{X})})$ and $Y = h_{\mathcal{Y}}(\tilde{Y}, Z^{(\mathcal{Y})})$.
- (c) The support $\text{supp } p_{\tilde{X}, \tilde{Y}} \subseteq \mathbb{R}^d \times \mathbb{R}^d$ of the distribution $p_{\tilde{X}, \tilde{Y}}$ is compact.
- (d) The pointwise mutual information $\text{PMI}_{\tilde{X}, \tilde{Y}}(\tilde{x}, \tilde{y}) := \frac{p_{\tilde{X}, \tilde{Y}}(\tilde{x}, \tilde{y})}{p_{\tilde{X}}(\tilde{x})p_{\tilde{Y}}(\tilde{y})}$ of \tilde{X} and \tilde{Y} is an L -Lipschitz function on $\text{supp } p_{\tilde{X}} \times \text{supp } p_{\tilde{Y}}$.

From the first and the second assumptions, it follows that there exists a 1-to-1 correspondence between (x, y) and $(\tilde{x}, \tilde{y}, z^{(\mathcal{X})}, z^{(\mathcal{Y})})$, and that $\frac{p_{X, Y}(x, y)}{p_X(x)p_Y(y)} = \frac{p_{\tilde{X}, \tilde{Y}}(\tilde{x}, \tilde{y})p_{Z^{(\mathcal{X})}}(z^{(\mathcal{X})})p_{Z^{(\mathcal{Y})}}(z^{(\mathcal{Y})})}{p_{\tilde{X}}(\tilde{x})p_{Z^{(\mathcal{X})}}(z^{(\mathcal{X})})p_{\tilde{Y}}(\tilde{y})p_{Z^{(\mathcal{Y})}}(z^{(\mathcal{Y})})} = \frac{p_{\tilde{X}, \tilde{Y}}(\tilde{x}, \tilde{y})}{p_{\tilde{X}}(\tilde{x})p_{\tilde{Y}}(\tilde{y})}$.

To show Theorem 5.1, we use the following statements.

Proposition C.3 ((Aronszajn, 1950; Sriperumbudur et al., 2011)). *Let X be a topological space. Let \mathcal{H} be a reproducing kernel Hilbert space of functions on X with $k: X \times X \rightarrow \mathbb{R}$ as its reproducing kernel. Then,*

$$\left\{ \sum_{j \in [n]} c_j k(\cdot, x_j) \mid n \in \mathbb{N}, \{c_j : j \in [n]\} \subset \mathbb{R}, \{x_j : j \in [n]\} \subset X \right\}$$

is dense in \mathcal{H} .

Lemma C.4. *Let X be a topological space. Let \mathcal{H} be a reproducing kernel Hilbert space of functions on X with a bounded kernel $k: X \times X \rightarrow \mathbb{R}$. Let $\sup_{x \in X} k(x, x) \leq \kappa$. For any $f, g \in \mathcal{H}$, if $\|f - g\|_{\mathcal{H}} < \varepsilon$, then $\|f - g\|_{\infty} < \sqrt{\kappa}\varepsilon$.*

Proof. For any $x \in X$,

$$|f(x) - g(x)| = \langle k(x, \cdot), f - g \rangle_{\mathcal{H}} \leq \|k(x, \cdot)\|_{\mathcal{H}} \|f - g\|_{\mathcal{H}} < \sqrt{\kappa}\varepsilon.$$

□

Definition C.5 (c_0 -universal, (Sriperumbudur et al., 2011)). A bounded kernel, k with $k(\cdot, x) \in C_0(X), \forall x \in X$ on a locally compact Hausdorff space, X is said to be c_0 -universal if the RKHS, \mathcal{H} induced by k is dense in $C_0(X)$ w.r.t. the uniform norm, i.e., for every function $g \in C_0(X)$ and all $\varepsilon > 0$, there exists an $f \in \mathcal{H}$ such that $\|f - g\|_{\infty} \leq \varepsilon$.

Proof of Theorem 5.1. First, we fix $\varepsilon > 0$. We show the statement by explicitly constructing $M^{(\mathcal{X})}, M^{(\mathcal{Y})}, f_{\mathcal{X}}$, and $f_{\mathcal{Y}}$ that satisfy Eq.16.

From (b) of Assumption C.2, there exist continuous inverse functions of $h_{\mathcal{X}}$ and $h_{\mathcal{Y}}$. Consider the following restrictions of the functions $h_{\mathcal{X}}^{-1}$ and $h_{\mathcal{Y}}^{-1}$: for $x = h_{\mathcal{X}}(\tilde{x}, z^{(\mathcal{X})})$ and $y = h_{\mathcal{Y}}(\tilde{y}, z^{(\mathcal{Y})})$, it holds that

$$\begin{aligned} \tilde{x} &= h_{\mathcal{X}}^{-1}|_{\tilde{X}}(x), \\ z^{(\mathcal{X})} &= h_{\mathcal{X}}^{-1}|_{Z^{(\mathcal{X})}}(x), \\ \tilde{y} &= h_{\mathcal{Y}}^{-1}|_{\tilde{Y}}(y), \\ z^{(\mathcal{Y})} &= h_{\mathcal{Y}}^{-1}|_{Z^{(\mathcal{Y})}}(y). \end{aligned}$$

Then, from (a) of Assumption C.2, it follows that

$$\begin{aligned} \frac{p_{X, Y}(x, y)}{p_X(x)p_Y(y)} &= \frac{p_{\tilde{X}, \tilde{Y}}(\tilde{x}, \tilde{y})p_{Z^{(\mathcal{X})}}(z^{(\mathcal{X})})p_{Z^{(\mathcal{Y})}}(z^{(\mathcal{Y})})}{p_{\tilde{X}}(\tilde{x})p_{Z^{(\mathcal{X})}}(z^{(\mathcal{X})})p_{\tilde{Y}}(\tilde{y})p_{Z^{(\mathcal{Y})}}(z^{(\mathcal{Y})})} \\ &= \frac{p_{\tilde{X}, \tilde{Y}}(\tilde{x}, \tilde{y})}{p_{\tilde{X}}(\tilde{x})p_{\tilde{Y}}(\tilde{y})} \\ &= \frac{p_{\tilde{X}, \tilde{Y}}(h_{\mathcal{X}}^{-1}|_{\tilde{X}}(x), h_{\mathcal{Y}}^{-1}|_{\tilde{Y}}(y))}{p_{\tilde{X}}(h_{\mathcal{X}}^{-1}|_{\tilde{X}}(x))p_{\tilde{Y}}(h_{\mathcal{Y}}^{-1}|_{\tilde{Y}}(y))}. \end{aligned} \tag{19}$$

To avoid complicated notations, we just denote $h_{\mathcal{X}}^{-1}|_{\tilde{\mathcal{X}}}(x)$ as $\tilde{x}(x)$ and $h_{\mathcal{Y}}^{-1}|_{\tilde{\mathcal{Y}}}(y)$ as $\tilde{y}(y)$ in the following.

From (c) of Assumption C.2, Proposition C.3, Lemma C.4, and the definition of c_0 -universal kernel, for any fixed $\tilde{y} \in \text{supp } p_{\tilde{\mathcal{Y}}}$, there exist $M \in \mathbb{N}$, $\{c_j \in \mathbb{R} \mid j \in [M]\}$ and $\{\tilde{\eta}_j \in \mathbb{R}^d \mid j \in [M]\}$ such that, for any $\tilde{x} \in \text{supp } p_{\tilde{\mathcal{X}}}$,

$$\left| \text{PMI}_{\tilde{\mathcal{X}}, \tilde{\mathcal{Y}}}(\tilde{x}, \tilde{y}) - \sum_{j \in [M]} c_j k(\tilde{x}, \tilde{\eta}_j) \right| < \frac{\varepsilon}{2}. \quad (20)$$

We denote such M, c_j , and $\tilde{\eta}_j$ as $M(\tilde{y}), c_j(\tilde{y})$ and $\tilde{\eta}_j(\tilde{y})$, respectively.

Meanwhile, we define $B_r(\tilde{y}) \subset \mathbb{R}^d$ as the open ball of radius r and center $\tilde{y} \in \mathbb{R}^d$. From (c) of Assumption C.2, the support of $p_{\tilde{\mathcal{Y}}}$ is compact. Thus, for any $\varepsilon > 0$, there exist $J \in \mathbb{N}$ and J points $\tilde{y}_1, \tilde{y}_2, \dots, \tilde{y}_J \in \mathbb{R}^d$ such that $\text{supp } p_{\tilde{\mathcal{Y}}} \subseteq \bigcup_{j=1}^J B_{\varepsilon/(2L)}(\tilde{y}_j)$. Given such \tilde{y}_j ($j \in [J]$), we define $\chi(\tilde{y})$ for $\tilde{y} \in S$ as one of the points, \tilde{y}_j ($j \in [J]$) that satisfies $\tilde{y} \in B_{\varepsilon/(2L)}(\tilde{y}_j)$. From (d) of Assumption C.2, it holds that, for any $(\tilde{x}, \tilde{y}) \in \text{supp } p_{\tilde{\mathcal{X}}, \tilde{\mathcal{Y}}}$,

$$\left| \text{PMI}_{\tilde{\mathcal{X}}, \tilde{\mathcal{Y}}}(\tilde{x}, \tilde{y}) - \text{PMI}_{\tilde{\mathcal{X}}, \tilde{\mathcal{Y}}}(\tilde{x}, \chi(\tilde{y})) \right| < \frac{\varepsilon}{2}. \quad (21)$$

Now, we are ready to construct desirable $M^{(\mathcal{X})}, M^{(\mathcal{Y})}, f_{\mathcal{X}}$ and $f_{\mathcal{Y}}$. Let $M^{(\mathcal{X})} = 1$ and $M^{(\mathcal{Y})} = \max_{j \in [J]} M(\tilde{y}_j)$. We define $f_{\mathcal{Y}} : y \mapsto \left\{ \left(w_j^{(\mathcal{Y})}, v_j^{(\mathcal{Y})} \right) \right\}_{j \in [M^{(\mathcal{Y})}]}$ as

$$\begin{aligned} w_j^{(\mathcal{Y})} &= c_j(\chi(\tilde{y}(y))) && \text{for } 1 \leq j \leq M(\chi(\tilde{y}(y))), \\ w_j^{(\mathcal{Y})} &= 0 && \text{for } M(\chi(\tilde{y}(y))) < j \leq M^{(\mathcal{Y})}, \\ v_j^{(\mathcal{Y})} &= \tilde{\eta}_j(\chi(\tilde{y}(y))) && \text{for } 1 \leq j \leq M(\chi(\tilde{y}(y))). \end{aligned}$$

For $v_j^{(\mathcal{Y})}$ with j such that $M(\chi(\tilde{y}(y))) < j \leq M^{(\mathcal{Y})}$, we can choose any point in \mathbb{R}^d . We define $f_{\mathcal{X}}$ as $f_{\mathcal{X}}(x) = \{(w_1, v_1)\} := \{(1, \tilde{x}(x))\}$. Then, we have that, for every $(x, y) \in \text{supp } p_{\mathcal{X}, \mathcal{Y}} \subseteq \mathcal{X} \times \mathcal{Y}$,

$$\begin{aligned} & \left| \ln \frac{p_{\mathcal{X}, \mathcal{Y}}(x, y)}{p_{\mathcal{X}}(x)p_{\mathcal{Y}}(y)} - \tilde{g}(f_{\mathcal{X}}(x), f_{\mathcal{Y}}(y)) \right| \\ &= \left| \text{PMI}_{\tilde{\mathcal{X}}, \tilde{\mathcal{Y}}}(\tilde{x}(x), \tilde{y}(y)) - \sum_{i=1}^{M^{(\mathcal{X})}} \sum_{j=1}^{M^{(\mathcal{Y})}} w_i^{(\mathcal{X})} w_j^{(\mathcal{Y})} k(v_i^{(\mathcal{X})}, v_j^{(\mathcal{Y})}) \right| \\ &\leq \left| \text{PMI}_{\tilde{\mathcal{X}}, \tilde{\mathcal{Y}}}(\tilde{x}(x), \tilde{y}(y)) - \text{PMI}_{\tilde{\mathcal{X}}, \tilde{\mathcal{Y}}}(\tilde{x}(x), \chi(\tilde{y}(y))) \right| \\ &\quad + \left| \text{PMI}_{\tilde{\mathcal{X}}, \tilde{\mathcal{Y}}}(\tilde{x}(x), \chi(\tilde{y}(y))) - \sum_{i=1}^{M^{(\mathcal{X})}} \sum_{j=1}^{M^{(\mathcal{Y})}} w_i^{(\mathcal{X})} w_j^{(\mathcal{Y})} k(v_i^{(\mathcal{X})}, v_j^{(\mathcal{Y})}) \right| \\ &\leq \frac{\varepsilon}{2} + \left| \text{PMI}_{\tilde{\mathcal{X}}, \tilde{\mathcal{Y}}}(\tilde{x}(x), \chi(\tilde{y}(y))) - \sum_{j=1}^{M(\chi(\tilde{y}(y)))} c_j(\chi(\tilde{y}(y))) k(\tilde{x}(x), \tilde{\eta}_j(\chi(\tilde{y}(y)))) \right| \\ &< \frac{\varepsilon}{2} + \frac{\varepsilon}{2} = \varepsilon. \end{aligned}$$

Here, the first inequality holds by the triangle inequality. The second inequality holds from Eq. 21 and the definition of $f_{\mathcal{X}}$ and $f_{\mathcal{Y}}$. The third inequality holds from Eq. 20. \square